Frontiers in Bioscience Landmark

Front. Biosci. (Landmark Ed) **2026**; 31(2): 48584
https://doi.org/10.31083/FBL48584

Original Research

Administering *Bifidobacterium pseudolongum* With Arsenic Trioxide Attenuates Acute Promyelocytic Leukemia in Mice by Restoring Immune Microenvironment and Intestinal Homeostasis

Zhibo Guo[1,2,3,†], Zengliang Gao[1,3,†], Yanqiu Zhao[2], Xiaoting Ni[1,4], Wenlei Zhang[1,3], Longyu Li[1,3], Shiao Ren[1,3], Qi Li[2], Dan Guo[2], Lijuan Yue[1,3], Yutong Liu[1,3], Liwang Lin[1,3], Shengjin Fan[2], Xin Hai[1,3,*]

[1]Department of Pharmacy, First Affiliated Hospital of Harbin Medical University, 150001 Harbin, Heilongjiang, China
[2]Department of Hematology, First Affiliated Hospital of Harbin Medical University, 150001 Harbin, Heilongjiang, China
[3]NHC Key Laboratory of Cell Transplantation, 150001 Harbin, Heilongjiang, China
[4]Department of Clinical Pharmacy, Qiqihar Medical University, 161006 Qiqihar, Heilongjiang, China
*Correspondence: haixin@hrbmu.edu.cn (Xin Hai)
[†]These authors contributed equally.
Academic Editor: Christian Borgo
Submitted: 26 November 2025 Revised: 31 December 2025 Accepted: 8 January 2026 Published: 5 February 2026

Abstract

Objective: Arsenic trioxide (ATO) is a cornerstone of acute promyelocytic leukemia (APL) therapy but induces severe gut microbiota dysbiosis, limiting its efficacy and safety. This study investigated whether adjunctive *Bifidobacterium pseudolongum* (BP) could mitigate these adverse effects and enhance therapeutic outcomes. **Methods**: 16S rRNA gene sequencing data of gut microbiota were obtained from a cohort of 22 APL patients treated with ATO-based regimens (20 of 22 data were obtained and analysis further), accessible under BioProject ID PRJNA935705. To evaluate the within-sample microbial community richness and evenness, alpha and beta diversity indices were calculated. Using a murine APL model, we compared ATO monotherapy with ATO+BP co-treatment. Analyses included fecal metagenomic sequencing, single-cell RNA sequencing (sc-RNA-seq), flow cytometric immune profiling, and assessment of intestinal tight junction proteins (claudin-1, occludin, and ZO-1) via immunofluorescence. **Results**: ATO treatment significantly reduced gut microbial diversity and depleted beneficial taxa. Sc-RNA-seq data showed that ATO could orchestrate the APL immune microenvironment mainly through functional activation of CD8+ T cells and monocytes. BP supplementation restored microbial homeostasis and synergistically enhanced ATO's antileukemic effect, reducing the leukemic burden in peripheral blood by 72% and in bone marrow by 64% compared to ATO alone. Mechanistically, BP preserved intestinal barrier integrity by upregulating tight junction protein expression and modulated anti-tumor immunity, notably increasing bone marrow CD8+ T cells by 2.21-fold. **Conclusions**: BP is an effective adjunct to ATO therapy, counteracting gut dysbiosis, intestinal damage, and the immune microenvironment while synergistically improving antileukemic efficacy. Targeting the gut–leukemia axis with BP represents a promising strategy for improving the precision and safety of APL treatment.

Keywords: arsenic trioxide; acute promyelocytic leukemia; intestinal homeostasis; bone marrow microenvironment; *Bifidobacterium pseudolongum*

1. Introduction

Arsenic trioxide (ATO), a derivative of arsenic, has revolutionized the treatment of acute promyelocytic leukemia (APL), a subtype of acute myeloid leukemia characterized by the promyelocytic leukemia–retinoic acid receptor α (*PML/RARα*) fusion gene [1]. APL arises from the t(15;17) chromosomal translocation, resulting in *PML/RARα*-mediated blockage of granulocyte differentiation. While ATRA/ATO combination therapy achieves high cure rates, 10–15% of patients relapse due to residual leukemic stem cells or acquired resistance [2,3]. Clinically, ATO induces apoptosis and promotes differentiation of leukemic promyelocytes by targeting the PML oncoprotein, achieving remission rates exceeding 90% when combined with all-trans retinoic acid (ATRA). Despite its efficacy, ATO therapy is associated with significant toxicities, including hematologic suppression [4], hepatotoxicity [5], and cardiac dysfunction [6], which limit its long-term use. Furthermore, emerging evidence suggests that arsenic disrupts intestinal homeostasis [7] and induces gut microbiota dysbiosis, which has been implicated in accelerating disease progression and promoting the onset of treatment-related complications [8]. These challenges underscore the need for strategies to mitigate ATO toxicity while preserving its antileukemic efficacy.

The gut microbiota plays a pivotal role in maintaining immune homeostasis and metabolic health [9,10]. A growing body of evidence indicates that the gut microbiota dysbiosis impairs therapeutic efficacy in various hematological

malignancies, including lymphoma [11] and leukemia [10, 12], and even influences outcomes following hematopoietic stem cell transplantation [13]. Chemotherapy and targeted therapies, including ATO, disrupt microbial diversity, leading to dysbiosis marked by reduced *Bifidobacterium* and *Lactobacillus* abundance and increased pathogenic *Enterococcus* and *Escherichia* species [8]. This imbalance compromises intestinal barrier integrity, increases systemic inflammation, and promotes leukemic cell survival through dysregulated cytokine production (e.g., TNF-α and IL-6) [14]. Notably, ATO-induced microbiota alterations correlate with heightened intestinal permeability, bacterial translocation, and subsequent hematopoietic suppression, creating a vicious cycle that exacerbates leukemia progression. Thus, restoring microbiota equilibrium represents a promising avenue to counteract therapy-related complications.

For APL, emerging resistance mechanisms include PML/RARα reactivation and epigenetic modifications that sustain leukemic cell survival [15]. Additionally, ATO's off-target effects on healthy tissues, particularly the gut, remain a critical barrier. Recent studies highlight the gut–liver axis in ATO metabolism, where dysbiosis exacerbates hepatic steatosis and drug toxicity, further complicating therapeutic outcomes [16]. Addressing these two challenges—enhancing efficacy and mitigating toxicity—requires innovative approaches targeting both leukemic cells and their microenvironment.

This study identifies *Bifidobacterium pseudolongum* (BP), a gut commensal with immunomodulatory properties, as a key protector for ATO related intestinal barrier integrity impairment and enhancer for therapeutic efficacy. In our investigation, BP attenuated ATO-induced intestinal barrier disruption by upregulating tight junction proteins (e.g., Claudin-1, Occludin, ZO-1). Murine model data demonstrate that BP co-administration with ATO reduced the APL cell burden. This dual therapeutic action positions BP as a novel adjunct to ATO therapy, addressing both efficacy and safety limitations in APL treatment. By elucidating BP's role in remodeling the gut–leukemia axis, this work bridges a critical gap in APL therapeutics. The integration of microbial with leukemia omics represents a paradigm shift, highlighting microbiota-targeted interventions as essential components of precision oncology.

2. Materials and Methods

2.1 Public Database Bioinformatics Analysis

To validate the impact of ATO on the human gut microbiota, a comprehensive bioinformatic re-analysis was performed using publicly available data from the National Center for Biotechnology Information (NCBI) Sequence Read Archive. Raw 16S rRNA gene sequencing data of gut microbiota were obtained from BioProject ID PRJNA935705, which included 22 APL patients receiving ATO-based regimens. 20 of 22 fecal samples data were obtained and further analyzed, including pre-treatment (APL group, n = 5) and post-ATO treatment (ATO group, n = 15). Raw sequencing data were processed using the QIIME 2 pipeline (version 2023.2, https://qiime2.org/). After quality control, denoising, and chimera removal via the DADA2 plugin, amplicon sequence variants (ASVs) were generated. Taxonomic classification was performed using the SILVA database (version 138.1, https://www.arb-silva.de/).

Alpha diversity indices, including Chao1 (species richness) and Shannon (richness and evenness), were calculated to assess within-sample diversity. Group differences were evaluated using the Mann–Whitney U test. Beta diversity was visualized using principal coordinate analysis (PCoA) based on weighted UniFrac distances. Differentially abundant bacterial genera between groups were identified using R package "DESeq2" (v1.38.3, https://www.bioconductor.org/packages/release/bioc/html/DESeq2.html). Spearman's rank correlation analysis was conducted among the top 10 most abundant genera, and a correlation heatmap was generated to explore interactions, especially involving key beneficial taxa such as *Bifidobacterium*.

2.2 Cell Culture and Reagents

The human APL cell line NB4 (ATCC® CRL-2047™) was cultured in RPMI-1640 (Gibco, Thermo Fisher Scientific, Waltham, MA, USA) supplemented with 10% fetal bovine serum (FBS; Gibco), 1% penicillin/streptomycin (Gibco), and 1% L-glutamine (Gibco) at 37 °C in a 5% CO_2 humidified incubator (Thermo Fisher Scientific, Waltham, MA, USA). ATO (GBW08666, purchased from the National Institute of Metrology, Beijing, China) was dissolved in sterile phosphate-buffered saline (PBS) to a final concentration of 200 µg/mL for *in vivo* assays. All cell lines were validated by STR profiling and tested negative for mycoplasma.

2.3 Murine APL Model and Bacterial Administration

Six-week-old female C57BL/6J mice were maintained under specific pathogen-free (SPF) conditions (22 $\pm$ 1 °C; 55% humidity; 12 h light/dark cycle). To establish an APL model, the mice received 450 cGy total-body irradiation (PRECISION X-RAY SmART+, Precision X-ray Inc, Madison, CT, USA) and were intravenously transplanted with 1 $\times$ 10^7 NB4 cells. After 20 days, successful engraftment was confirmed by peripheral blood smear analysis via tail vein sampling and defined as $\geq$20% leukemic cells by microscopy. Subsequently, the mice were treated with ATO $\pm$ BP bacteria: BP (BeNa Culture Collection, BNCC135158, Beijing, China; 1 $\times$ 10^9 CFU/mL, 200 µL/dose orally, thrice weekly) and ATO (1 mg/kg, intraperitoneal injection, daily for 14 days) were co-administered for 14 days. Control groups included APL mice receiving PBS alone. Mice were euthanized by pentobarbital sodium = 100 mg/kg and monitored for loss of the righting

reflex and corneal reflex. Once unresponsive, euthanasia was immediately performed by cervical dislocation; death was confirmed by the absence of respiration, palpable heartbeat, and pupillary light reflex. All manipulations were conducted by trained personnel using appropriate personal protective equipment (PPE; e.g., gloves, lab coat, eye protection) and aseptic technique. After confirmed death, orbital sinus blood was collected in a non-survival procedure. The animal was placed in lateral recumbency, and the medial canthus and periorbital skin were disinfected with 75% ethanol. A sterile, blunt-ended capillary tube (0.5 × 100 mm) was inserted at a 30°–45° angle relative to the nasal plane, advanced approximately 2–3 mm along the posterior orbital wall until resistance was felt, then gently rotated ~180° to lacerate the orbital venous plexus. Blood was collected by capillary action into EDTA-coated microtubes. Tibiae, spleen and colon were collected for subsequent studies, with details described later. All steps complied with the AVMA Guidelines and were approved by the Institutional Animal Ethics Committee of the First Affiliated Hospital of Harbin Medical University (IACUC No.2025032).

2.4 Fecal Metagenomics and Gut Microbiota Analysis

Fecal samples were collected from mice in the ATO and ATO+BP groups (n = 8 per group). Genomic DNA was extracted using the DP328 Fecal Genomic DNA Extraction Kit (Centrifugal Column Type, TIANGEN, Beijing, China), and DNA quality was assessed based on 260/280 nm and 260/230 nm absorbance ratios.

Library preparation was performed using the Rapid Plus DNA Library Prep Kit for Illumina (RK20208, ABclonal, Wuhan, China). DNA fragmentation was carried out with a Covaris LE220R-plus Ultrasonicator (Covaris, Woburn, MA, USA), and sequencing was conducted on an Illumina NovaSeq X Plus System (PE150, Illumina, San Diego, CA, USA).

Following ATO treatment, alpha diversity (Chao1, Shannon, and Simpson) and beta diversity (Bray–Curtis dissimilarity) indices were calculated to assess microbial community richness, evenness, and structural variation.

2.5 Cell Isolation and Single-Cell RNA-Seq Analysis

Bone marrow aspirates were collected from tibial bone marrow cavities using 1× DPBS (Thermo Fisher Scientific, 14190144) supplemented with 10 µg/mL DNase I (Sigma-Aldrich, 11284932001) on ice. Cell suspensions were filtered through 40 µm nylon cell strainers (Corning Incorporated, Corning, NY, USA, 352340) and treated with 1× Red Blood Cell Lysis Solution (Thermo Fisher Scientific, 00-4333-57) to eliminate erythrocytes. After washing with 1× DPBS containing 2% fetal bovine serum (FBS; Gibco, 10082147), cell viability was assessed using 0.4% Trypan Blue (Thermo Fisher Scientific, 14190144) via Countess® II Automated Cell Counter (Thermo Fisher Scientific).

CD11b immune cells were isolated using CD45 microbeads and MACS LS columns (Miltenyi Biotec, Bergisch Gladbach, Germany, 130-042-301) following the manufacturer's protocol. Single-cell libraries were generated using the 10× Genomics Chromium Next GEM Single Cell 3′ Kit v3.1 (10× Genomics, Pleasanton, CA, USA, 1000121) according to the CG000206 Rev D protocol. Briefly, cells were partitioned into droplets using the Chromium Controller, followed by reverse transcription, cDNA amplification, and library preparation. Final libraries were quantified via High Sensitivity DNA Analysis (Agilent Bioanalyzer 2100, Agilent Technologies, Santa Clara, CA, USA) and Qubit dsDNA HS Assay (Thermo Fisher Scientific), then sequenced on an Illumina NovaSeq 6000 platform (2 × 150 bp paired-end configuration).

Raw reads were processed using Cell Ranger v2.1.0 (10× Genomics) with default parameters for alignment to the GRCm38 mouse genome (STAR aligner v2.7.8a, https://github.com/alexdobin/STAR). Gene-barcode matrices were generated after Unique Molecular Identifier (UMI) counting and barcode filtering. Data integration and batch correction were performed by R package "Seurat" (version 2.3.0, https://cran.r-project.org/web/packages/Seurat/index.html).

The normalized data (NormalizeData function in Seurat package) was performed for extracting a subset of variable genes. Variable genes were identified while controlling for the strong relationship between variability and average expression. Next, we integrated data from different samples after identifying "anchors" between datasets using FindIntegrationAnchors and IntegrateData in the Seurat package. The clusters were visualized by Uniform Manifold Approximation and Projection (UMAP). In order to understand the BMME in APL, HALLMARK analysis was used to evaluate immune cells in samples [17]. The difference in the abundance of immune cell infiltration was analyzed.

2.6 Histopathology

Spleens and distal colons were fixed in 10% neutral-buffered formalin (Leica Biosystems, Nussloch, Germany) for 24–48 h, processed routinely, embedded in paraffin, and sectioned at 5 µm. Sections were stained with hematoxylin and eosin (H&E) for histopathological evaluation or subjected to immunohistochemistry (IHC) for Ki67 detection (DAKO, Glostrup, Denmark).

For immunofluorescence (IF), paraffin-embedded sections were deparaffinized, rehydrated, and subjected to antigen retrieval (citrate buffer, pH 6.0, 95 °C for 20 min). After blocking, sections were incubated with primary and fluorescent-conjugated secondary antibodies, followed by DAPI counterstaining. Fluorescence microscopy images were acquired using a Zeiss AXIO Imager M2 system (ZEISS, Oberkochen, Denmark), while bright-field (white light) images were captured using an Olympus CKX53 microscope (OLYMPUS, Tokyo, Japan). Antibody pan-

els including anti-Ki67 antibody (DAKO, Glostrup, Denmark, 1:200) and, for immunofluorescence, Claudin-1 (Servicebio, Wuhan, China, GB11032, 1:500), Occludin (Abcam, Cambridge, UK, ab53032, 1:500), and ZO-1 (Servicebio, Wuhan, China, GB111402, 1:500) were employed. Secondary antibodies (ZSGB-BIO, Beijing, China) and all reagents were prepared following the manufacturers' instructions.

2.7 Flow Cytometry (FCM)

Bone marrow cells were isolated by flushing the bilateral tibiae and femurs with PBS supplemented with 2% FBS, followed by filtration through a 70 µm nylon mesh for FCM analysis. Bone marrow and peripheral blood cells were treated with red blood cell (RBC) lysis buffer and then filtered through 70 µm nylon strainers (BD Falcon, Franklin Lakes, NJ, USA). Antibodies for FCM were purchased from Thermo Fisher Scientific, MA, USA. The panels included (1) APL cells: anti-hCD11b (11-0118-42) and hCD33 (12-0339-42); (2) monocytes: anti-mCD11b (12-0112-81) and Ly6C (53-5932-82); (3) T cells: anti-mCD3 (11-0032-80), CD8 (17-0081-82), and CD4 (12-0041-81). Each panel included the live/dead stain eBioscience™ Fixable Viability Dye eFluor™ 780 (65-0865-14). Data were acquired on a BD FACSCanto™ II (Becton, Dickinson and Company, NJ, USA) and analyzed using FlowJo software (version 10.8.1, https://www.flowjo.com) .

2.8 Statistical Analysis

Data are presented as mean ± SEM. Normality was assessed via the Shapiro–Wilk test. Parametric comparisons used Student's *t*-test (two groups) or one-way ANOVA with Tukey's post hoc (multiple groups). Non-parametric data were analyzed by the Mann–Whitney U test. Permutational multivariate analysis of variance (PERMANOVA) was used to test for significant compositional differences between groups in PCoA analysis. The PERMANOVA results were obtained based on Euclidean distance with 9999 permutations. Correlations were evaluated via Spearman's rank (α = 0.05). Statistical software included GraphPad Prism (version 10.1.0, https://www.graphpad.com/) and R (version 4.3.1, https://cran.r-project.org/). For microbiota analysis, DESeq2 (v1.38.3) was used to obtain normalized raw counts, and taxonomic profiling was performed using SILVA 138.1. Raw and processed data are available in the NCBI Sequence Read Archive and the corresponding author's institutional repository.

3. Results

3.1 ATO Treatment Disrupts the Gut Microbiota in APL Patients

Building upon previous reports [8], we analyzed 16S rRNA sequencing data from 20 APL patients treated with ATO based regimens (BioProject ID: PRJNA935705). Our analysis revealed that ATO therapy induced significant alterations in gut microbiota composition, including reduced microbial diversity and depletion of beneficial taxa such as *Bifidobacterium*. A significant difference in Shannon diversity was observed between ATO-based treatment patients (ATO group) and the non-treated group (APL group), which demonstrated a significantly lower diversity in the feces of ATO group (Fig. 1A). Principal coordinate analysis (PCoA) demonstrated a significant difference in β-diversity using the weighted UniFrac distance between the ATO and APL groups, suggesting that the microbial composition in APL patients was significantly shifted regarding operational taxonomic units (OTUs) (Fig. 1B). Notably, the abundance of beneficial gut microbiota—including *Romboutsia*, *Blautia*, and *Bifidobacterium*—was significantly decreased following ATO treatment (Fig. 1C), and Spearman correlation analysis further revealed an inverse association between *Bifidobacterium* and other probiotic taxa (Fig. 1D); these findings raise two critical questions: whether the reduction in these protective bacterial populations is mechanistically linked to the therapeutic efficacy of ATO, and whether similar microbiota alterations occur in animal models where ATO's pharmacological effects are well-characterized.

3.2 ATO-Induced Dysbiosis in a Murine APL Model

To investigate whether ATO affects the gut microbiota in murine models, we established an APL mouse model and collected fecal samples from both ATO-treated (ATO group) and control (APL group) mice before euthanasia (Fig. 2A). A total of 16 fecal samples (8 per group) were subjected to metagenomic sequencing. Consistent with the human data, murine APL models recapitulated similar dysbiotic patterns. ATO-treated mice showed a relative reduction in OTUs compared to controls (Fig. 2B–D). Principal component analysis (PCA) of UniFrac distances confirmed microbiota shifts (Fig. 2E), and the heatmap showed a decrease in *Bifidobacterium* abundance, especially BP (Fig. 2F).

3.3 BP Administration Enhances APL Treatment Effectiveness in Mice

Although LEfSe analysis did not identify significant abnormalities based on our metagenomic sequencing data, we observed abundance differences of BP after ATO treatment, consistent with evidence from the previous literature suggest that ATO treatment markedly reduces *Bifidobacterium* abundance [8]. To investigate the functional role of BP bacteria during ATO therapy, we supplemented ATO administration with BP. After 14 days of treatment, bone marrow and peripheral blood samples were collected for FCM analysis (Fig. 3A). Notably, the combination of BP supplementation and ATO (BP+ATO) significantly reduced APL cell burden. Specifically, in ATO+BP-treated mice, peripheral blood leukemic blasts were reduced by 72% (4.57% ± 0.49% vs. 16.53% ± 7.09%; p = 0.043) (Fig. 3B), while

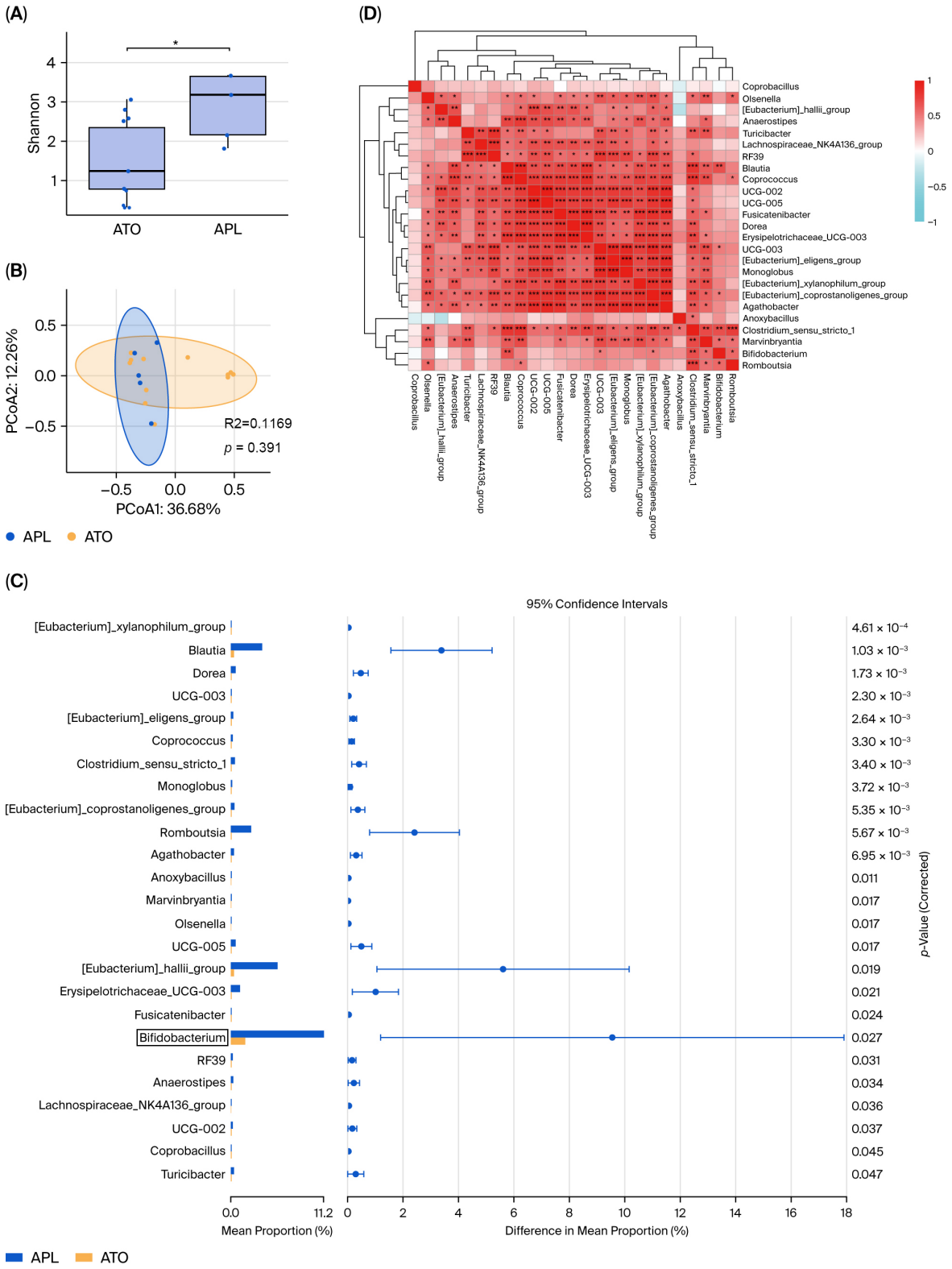

Fig. 1. The diversity and composition of the gut microbiota are significantly altered in APL patients after treatment with ATO. Data of 16S rRNA genes sequenced from APL patients after or before ATO treatment. (A) The diversity and richness of the gut microbiota in APL patients before (APL n = 5) and after ATO treatment (ATO n = 15). (B) PCoA of a weighted UniFrac distance analysis (n = 20), $R^2 = 0.1169$, $p = 0.0391$. (C) Relative taxon abundance comparison among the APL and ATO groups, with *Bifidobacterium* showing a significant change (n = 17). (D) Spearman correlations between the intestinal content of the 10 genera in the APL and ATO groups (red: positive correlation; blue: negative correlation). *: $p < 0.05$, **: $p < 0.01$, ***: $p < 0.001$. APL, acute promyelocytic leukemia; ATO, arsenic trioxide; PCoA, principal coordinate analysis.

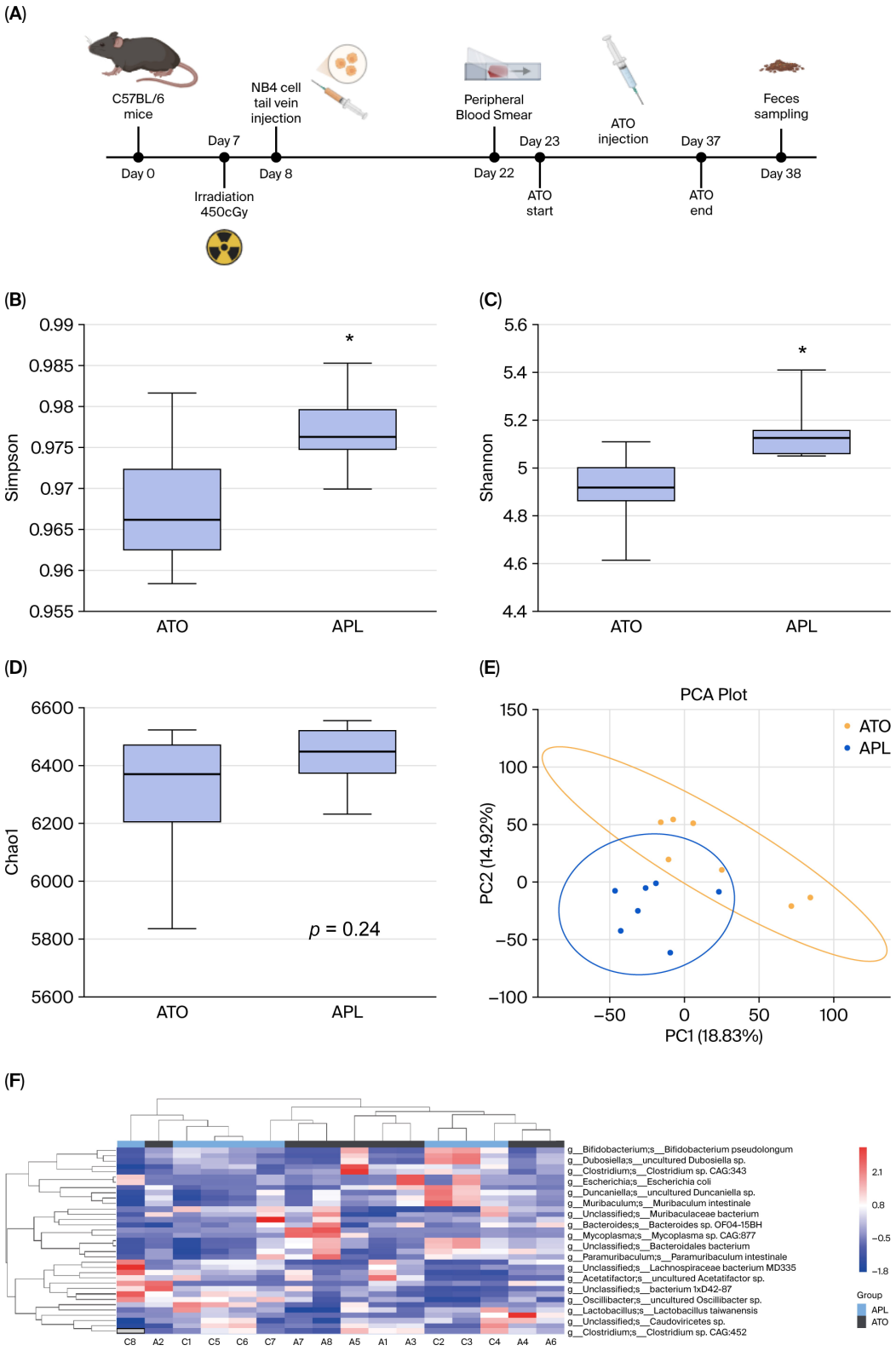

Fig. 2. The diversity and composition of the gut microbiota are significantly altered in APL mouse models after treatment with ATO. (A) Schematic diagram of the mouse experimental process. (B–D) Alpha and beta diversity based on data of bacterial metagenomics from APL murine models after or before ATO treatment (n = 8, respectively), *$p < 0.05$ *vs.* ATO. (E) PCA of a weighted UniFrac distance analysis (n = 8, respectively). (F) The heatmap indicates a significant reduction in the abundance of BP after ATO treatment. PCA, principal component analysis.

in bone marrow (CD11b±/CD33+), they were reduced by 64% (2.76% ± 0.94% vs. 7.39% ± 1.07%; $p = 0.005$) (Fig. 3C). Histopathological analysis of spleens revealed fewer leukemic infiltrates in the ATO+BP group (Fig. 3D). These findings collectively indicate that BP supplementation synergistically enhances the therapeutic efficacy of ATO against APL in murine models.

3.4 ATO Orchestrates the APL Immune Microenvironment Mainly Through Functional Activation of CD8+ T Cells and Monocytes

Here, we conducted paired scRNA-seq and scTCR/BCR-seq profiling on 6 bone marrow (BM) aspirates (3 with and 3 without ATO) (Fig. 4A). As the mice had undergone irradiation prior to leukemia cell inoculation, both groups exhibited markedly low hematopoietic stem cell (HSC) proportions compared to clinical APL patients. ATO treatment induced profound remodeling of the immune microenvironment. Unsupervised immune cell clustering and scoring revealed widespread transcriptional alterations across major immune populations (Fig. 4B,C). Notably, while CD8+ T cells showed reduced abundance, post-ATO treatment. This depletion might reflect exhaustion following APL remission, suggesting that strategies to preserve or expand CD8+ T cells could amplify ATO's immunotherapeutic efficacy. In contrast, B cells and basophils remained stable. HALLMARK analysis demonstrated commonly enhanced inflammatory responses especially in neutrophilsm monocytes and CD8+ T cells (Fig. 4D).

3.5 BP Modulates the Immune Microenvironment and Intestinal Barrier Function in Mice

Previous studies have demonstrated that probiotics can mitigate intestinal barrier dysfunction caused by pathological conditions or pharmacological interventions [8,10, 18]. In this study, we investigated whether BP supplementation could counteract ATO-induced intestinal barrier impairment. Using immunofluorescence analysis, we quantified the expression of tight junction proteins (Claudin-1, Occludin, and ZO-1) in colonic epithelial cells. ATO treatment alone compromised intestinal barrier function, as evidenced by the decreased expression of tight junction proteins Claudin-1, Occludin, and ZO-1 (Fig. 5A, **Supplementary Fig. 1A–C**). Strikingly, BP supplementation in ATO-treated mice restored tight junction integrity, as shown in Fig. 5A. Interestingly, previous studies have demonstrated that BP bacteria modulate the tumor microenvironment, particularly by increasing CD8+ T cell proportions and enhancing antitumor immunity [19]. Consistently, our flow cytometry analysis of peripheral blood and bone marrow from ATO ± BP-treated mice revealed that BP co-administration significantly elevated monocyte and CD8+ T cell frequencies as FCM results shown. Monocytes exhibited the most pronounced alteration, demonstrated by a 1.42-fold increase in peripheral blood (71.90% ± 6.25% vs. 48.47% ± 4.51%; $p = 0.006$; Fig. 5B) and a 2.18-fold expansion in bone marrow (16.23% ± 5.95% vs. 7.44% ± 1.48%; $p = 0.068$; Fig. 5C). Notably, despite their low abundance, BP co-treatment significantly modulated CD8+ T cell numbers; in peripheral blood, there was a 1.69-fold increase (1.69% ± 0.12% vs. 0.99% ± 0.24%; $p = 0.012$; Fig. 5D) and in bone marrow a 2.21-fold elevation (3.18% ± 0.52% vs. 1.43% ± 0.38%; $p = 0.009$; Fig. 5E).

4. Discussion

In this study, we systematically investigated the synergistic effects of ATO and BP in treating APL, with a focus on mitigating ATO-induced intestinal dysbiosis and enhancing therapeutic efficacy. Using integrated *in vitro*, *in vivo*, and multi-omics approaches, we demonstrated that BP administration restored gut barrier integrity, modulated the immune microenvironment, and amplified ATO-induced leukemic cell apoptosis. Key findings included (1) ATO-induced microbiota dysbiosis characterized by *Bifidobacterium* depletion and pathogenic taxa expansion; (2) ATO orchestrates the APL immune microenvironment mainly by activating CD8+ T cells and monocytes; (3) BP-mediated restoration of tight junction protein (Claudin-1, Occludin, and ZO-1) production; and (4) BP increased the amount of CD8+ T cells and monocytes to remodel microenvironment (Fig. 6). These results position BP as a novel adjunct to ATO therapy, addressing both efficacy and toxicity challenges in APL treatment.

While ATO combined with ATRA achieves >90% remission rates in APL, its non-selective toxicity (e.g., intestinal mucositis) remains a critical barrier [20]. Our findings align with prior studies highlighting ATO-induced dysbiosis as a driver of systemic toxicity. This study bridges a critical gap in APL therapeutics by integrating microbiota with leukemia omics, a paradigm underexplored in previous APL trials. Current exploration of ATO's therapeutic mechanisms includes fusion genes [21,22], epigenetics [23], and transport proteins [24,25]. In contrast, the role of tumor microenvironment and inter-organ interactions has received limited attention despite its importance.

BP is an anaerobic, Gram-positive probiotic bacterium within the *Bifidobacterium* genus that ferments sugars to produce lactic acid and acetate, while synthesizing various metabolites including L-arginine and short-chain fatty acids, synergistic exerting multiple anti-inflammatory and tumor effects [19,26]. Intestinal barrier impairment exacerbates inflammation through inflammatory cytokines that might promote tumor progression [27]. Our scRNA-seq and flow cytometry analyses demonstrated that ATO activates cytotoxic CD8+ T cells and monocytes, while BP further expands CD8+ T cell frequencies in bone marrow (2.21-fold increase). These results directly support BP's role in modulating anti-leukemic immunity. As crucial components of the immune system, CD8+ T cells influence

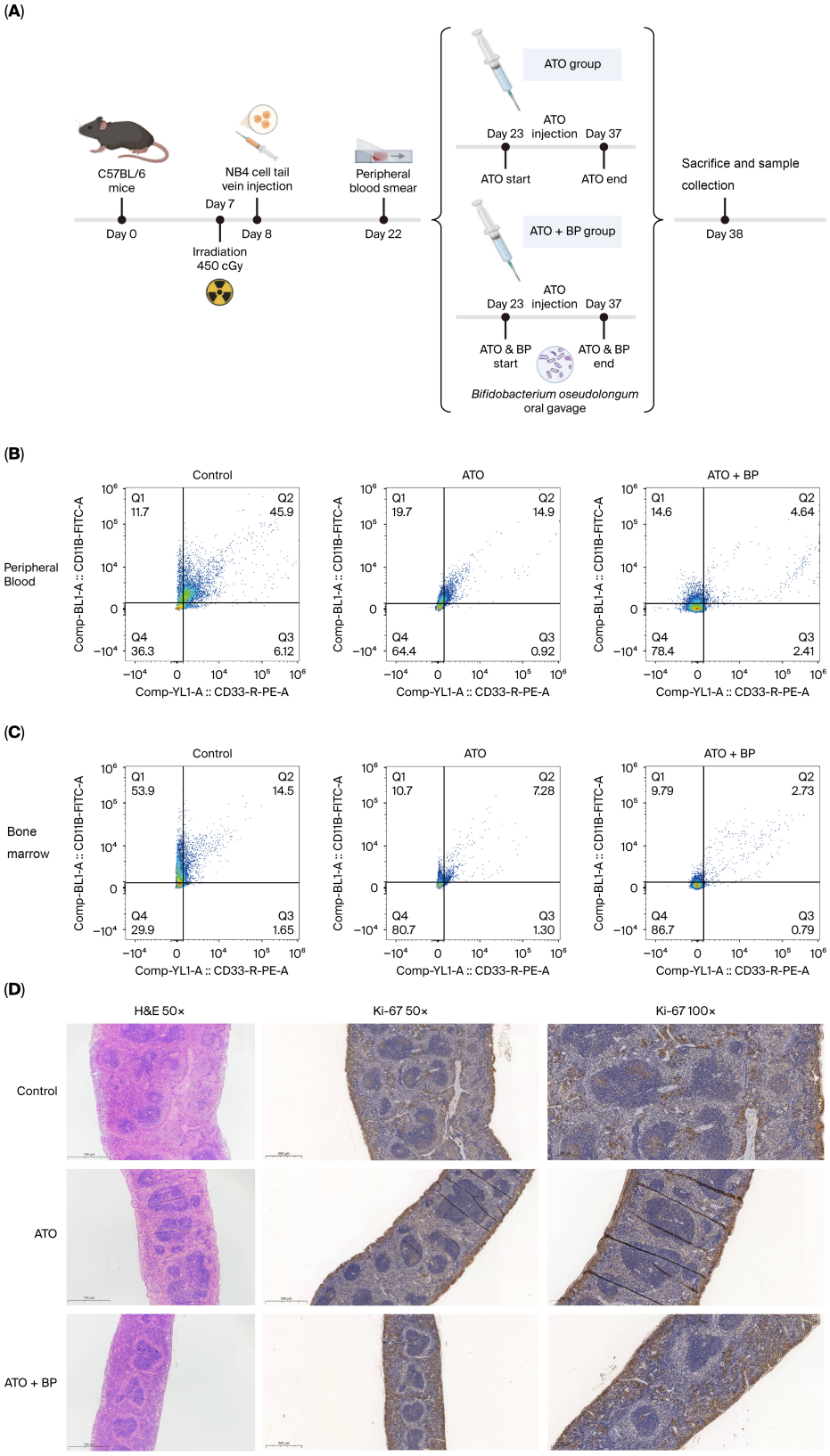

Fig. 3. BP alleviated APL cell burden in mouse models. (A) Schematic diagram of the mouse experimental process. (B)Leukemia cells (CD11b+/CD33+ cells) in peripheral blood from ATO mice (n = 4) and ATO+BP mice (n = 4). $p = 0.043$. (C) Leukemia cells (CD11b+/CD33+ cells) in bone marrow from ATO mice (n = 4) and ATO+BP mice (n = 4). $p = 0.005$. (D) H&E histopathology sections and Ki-67 IHC of a representative spleen: control, ATO group, and ATO+BP group. All microscopic analyses were performed (Scale bar = 500 μm, left and middle; scale bar = 200 μm, right). BP, *Bifidobacterium pseudolongum*; H&E, hematoxylin and eosin.

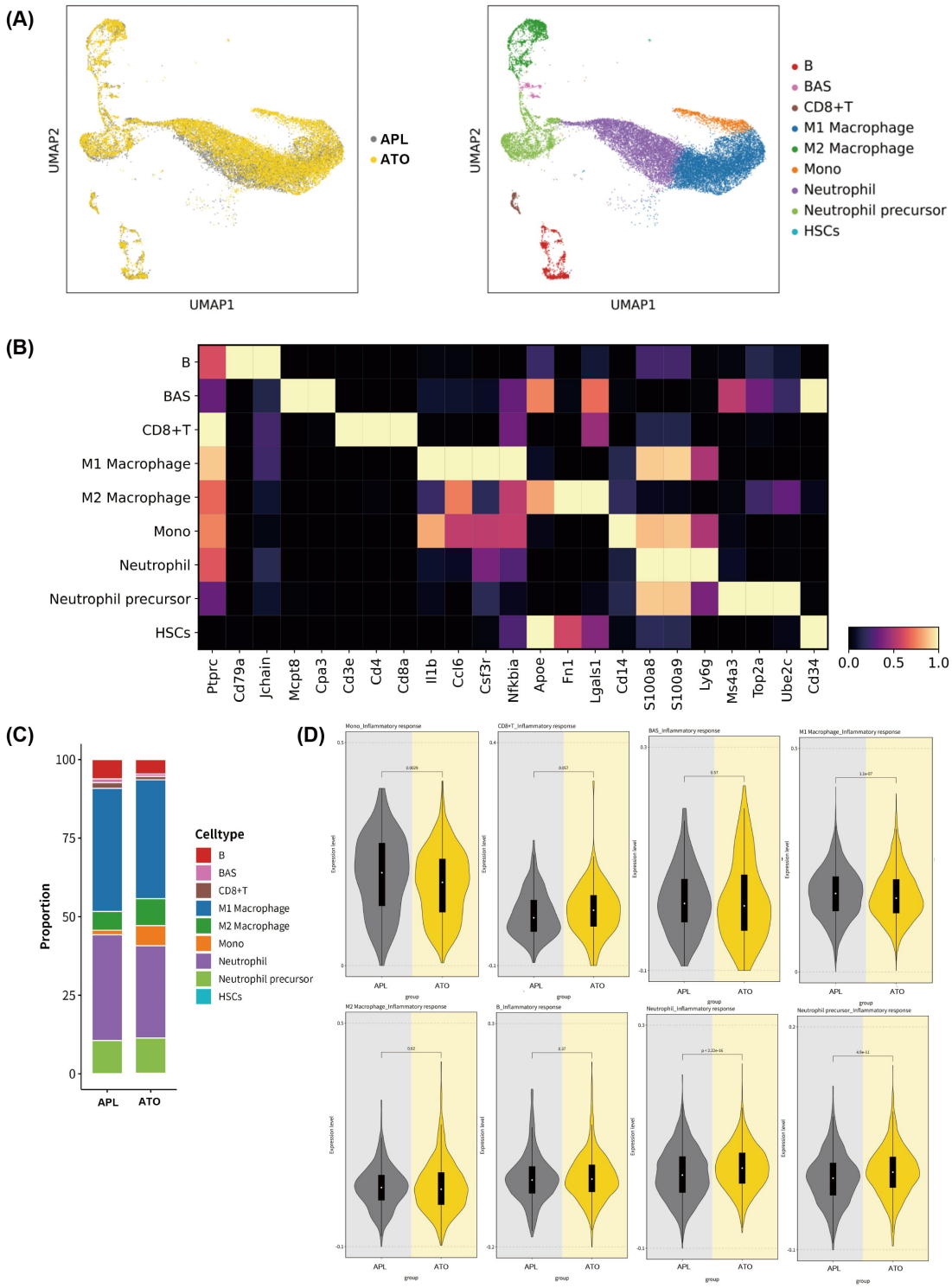

Fig. 4. Landscape of Microenvironment in APL murine models with ATO treatment by single-cell RNA sequencing and the functional states of APL subtypes. (A) UMAP plot of BM samples from murine models with or without ATO. (B) Heatmap showing the scaled expression levels of genes in specific subtypes. (C) Proportion comparison of cell fraction between APL and ATO group. (D) Comparative immunophenotypic analysis of ATO-treated versus untreated mice revealed distinct immune modulation patterns. ATO administration induced significant immunomodulatory effects across multiple immune cell subsets: monocytes: $p = 0.0029$, CD8+ T cells: $p = 0.057$, BAS: $p = 0.57$, M1 macrophages: $p = 1.1 \times 10^{-7}$, M2 macrophages: $p = 0.62$, B cells: $p = 0.37$, Neutrophils: $p = 2.2 \times 10^{-16}$ and Neutrophil precursor: $p = 4.9 \times 10^{-11}$. UMAP, Uniform Manifold Approximation and Projection; BM, bone marrow; BAS, Basophil.

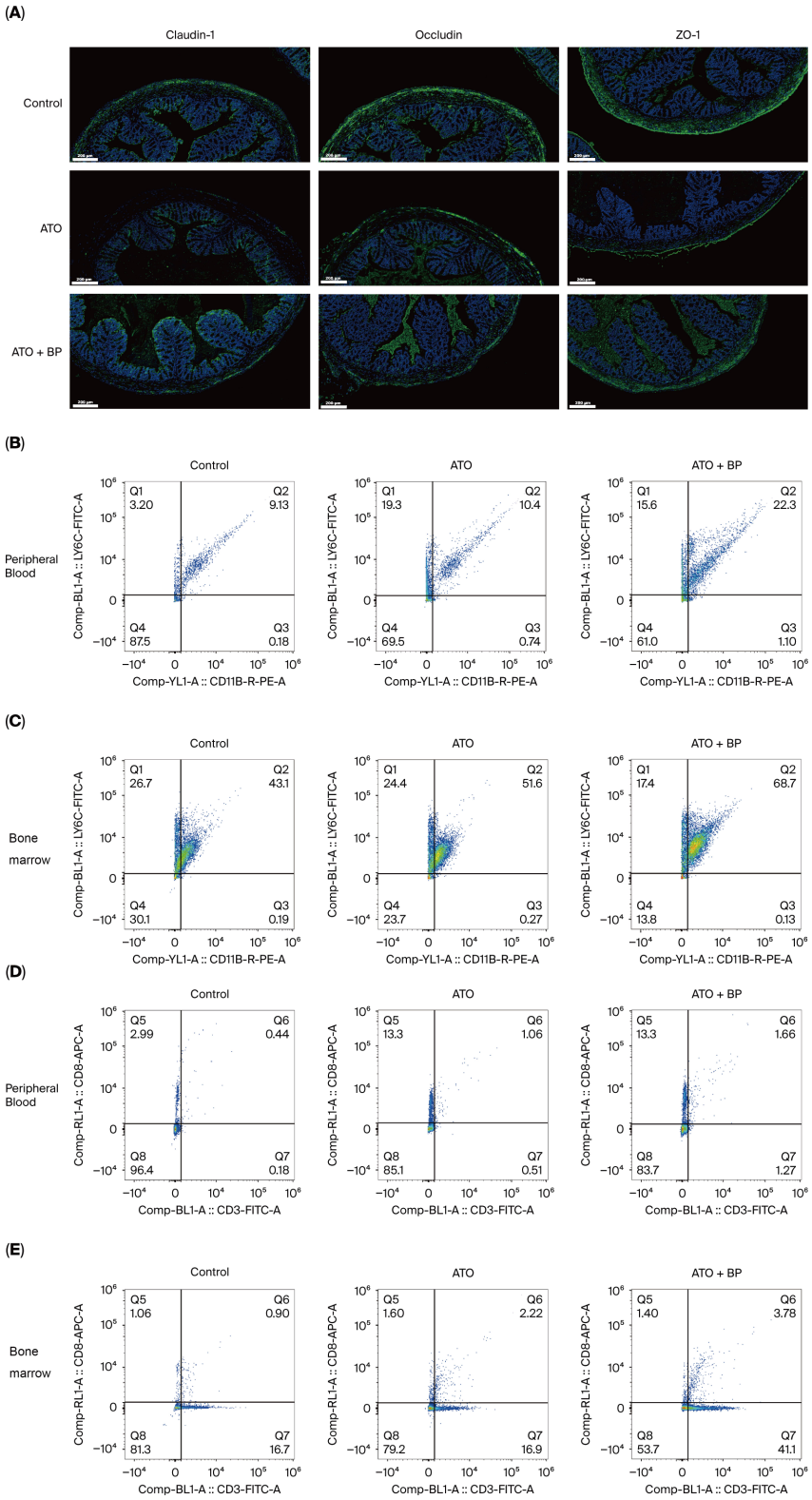

Fig. 5. BP remodeled the immune microenvironment and repaired the intestinal barrier in murine models. (A) Representative IF images showing Claudin-1, Occludin, and ZO-1 (all in green) localization with DAPI nuclear counterstain (blue) (n = 4 per group), quantification data were shown in **Supplementary Fig. 1**. Scale bar: 200 μm. (B) Monocytes (CD11b+Ly6c+ cells) in peripheral blood from ATO mice (n = 4) and ATO+BP mice (n = 4). $p = 0.006$. (C) Monocytes (CD11b+Ly6c+ cells) in bone marrow from ATO mice (n = 4) and ATO+BP mice (n = 4). $p = 0.068$. (D) CD8+ T cells (CD3+/CD8+ cells) in peripheral blood from ATO mice (n = 4) and ATO+BP mice (n = 4). $p = 0.012$. (E) CD8+ T cells (CD3+/CD8+ cells) in bone marrow from ATO mice (n = 4) and ATO+BP mice (n = 4). $p = 0.009$. IF, immunofluorescence; DAPI, 4′,6-diamidino-2-phenylindole.

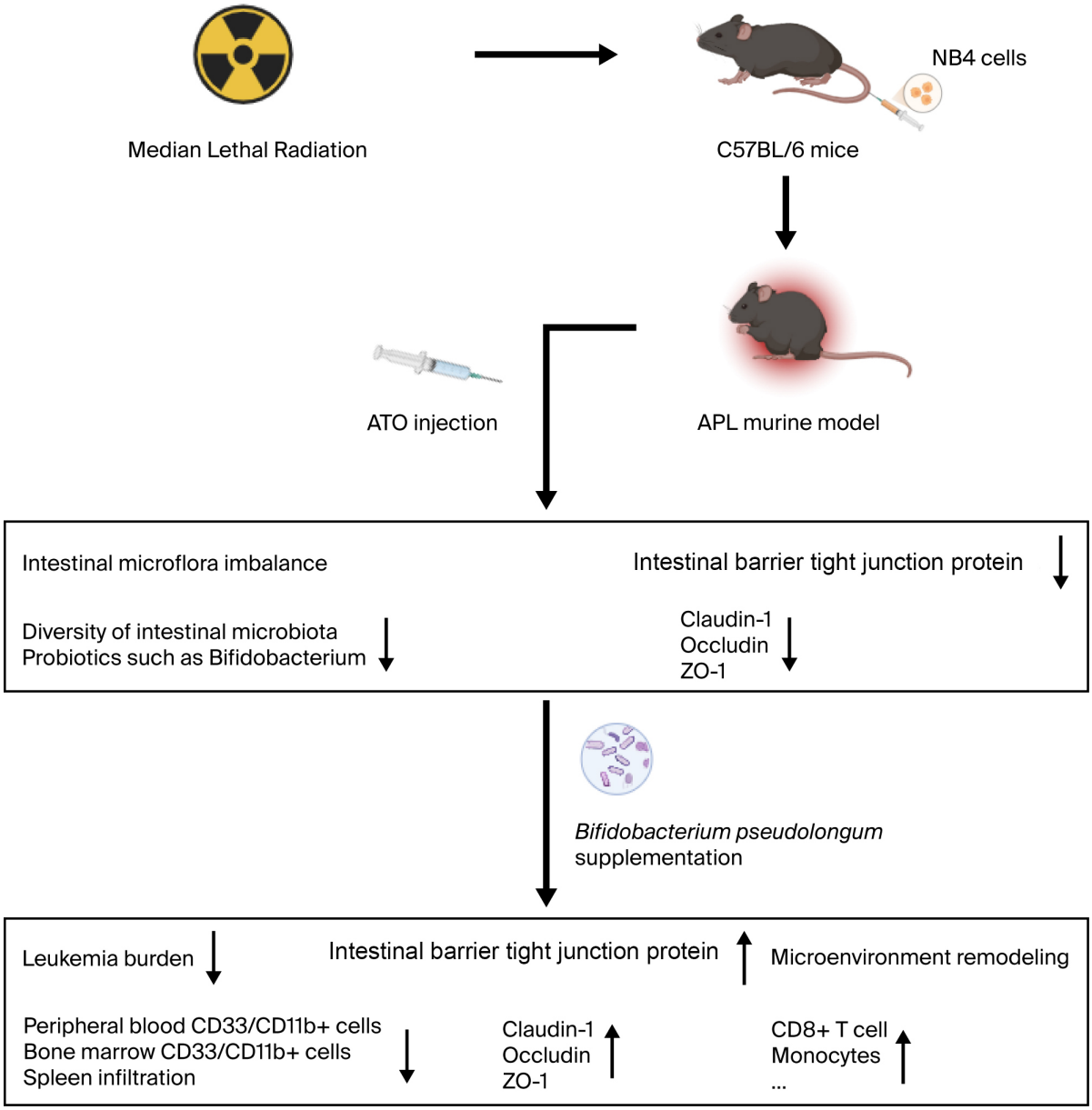

Fig. 6. Impact of ATO on intestinal microbiota and tissue damage in mice, with BP supplementation alleviating toxicity and potentiating drug efficacy. ↑: increase protein expression or cell counts, ↓: decrease protein expression or cell counts. The schematic diagrams were created using the BioRender website (https://app.biorender.com/).

the therapeutic efficacy of AML treatment [28–30], which serve as pivotal effectors in adaptive anti-tumor immunity [31–33]. Tumor-infiltrating CD8+ T cell density correlates positively with improved prognosis across multiple cancers [34–36]. Supplementing BP further enhances CD8+ T cell proliferation to exert anti-tumor effects. Previous studies propose that CD8+ T cells facilitate monocyte infiltration [37]. In our study, BP cooperates with ATO to enhance CD8+ T cell effector function. The reciprocal interaction between these immune cells presents a fascinating area worthy of in-depth investigation [38].

This study has several limitations that should be acknowledged. First, the murine cohort and limited human microbiota data may restrict the generalizability of findings, with the confounding factors could not be ruled out yet, necessitating validation in larger, more diverse cohorts. Comparing the roles of BP and other Bifidobacteria in the treatment of APL would be also an interesting topic for future research. And the contributions of direct microbial anti-leukemic effects and ATO pharmacokinetics cannot be ruled out and warrant further investigation. Second, the irradiation (450 cGy) used in our murine model likely contributed to transient lymphopenia [39], a limitation inherent to preclinical APL studies. Moreover, the use of lethally irradiated mice to establish APL models, while critical for leukemia engraftment, introduces

confounding factors such as radiation-induced immunosuppression and other lesions, which may not fully recapitulate human APL microenvironment. Future studies will further investigate the effects of ATO and BP on the immune microenvironment using immunocompetent animal models. Third, direct metabolomic validation in intestinal epithelial cells or leukemia blasts remains unexplored, leaving mechanistic gaps in how BP modulates host–microbe interactions. Current studies confirm BP repairs the intestinal barrier via immunofluorescence (Claudin-1, Occludin, and ZO-1). These functional validations—independent of metabolomics—demonstrate BP indirectly modulates host-microbe interactions by restoring barrier integrity. While metabolomics uncovers molecular details, it is complementary: key findings (e.g., immune reprogramming) are already validated via flow cytometry (CD8+ T cell expansion) and microbiome analysis. We will further conduct immune cell depletion studies to strengthen causal inference. Fourth, the therapeutic window and long-term safety of BP supplementation in APL patients, particularly its impact on gut barrier integrity during ATO-induced mucositis, require further investigation. We also need to evaluate the survival benefit and safety of probiotics in immunocompromised hosts. Finally, the absence of immune checkpoint inhibitor co-therapy in our model limits insights into BP's role in synergizing with modern immunotherapies, highlighting a critical avenue for future research.

This work provides a foundation for optimizing ATO-based APL therapy through microbiota modulation. Mechanistically, targeting the gut–leukemia axis offers a dual benefit: enhancing leukemia cell apoptosis while preserving intestinal homeostasis. Future trials should evaluate BP as an adjunct to ATO regimens, particularly in high-risk APL patients with baseline dysbiosis. Additionally, integrating BP with fecal microbiota transplantation or engineered probiotics could further personalize therapy. By addressing both efficacy and toxicity, this strategy aligns with the evolving paradigm of "precision oncology" , where microbial interventions complement conventional therapies.

5. Conclusions

This study reveals that ATO therapy disrupts gut microbiota balance in APL by depleting *Bifidobacterium*, exacerbating intestinal permeability and restoring microenvironment. Co-administration of BP restores microbial diversity, enhances gut barrier integrity, and synergizes with ATO in rewiring microenvironment to reduce leukemic burden.

Availability of Data and Materials

The datasets used and analyzed during the current study are available from the corresponding author on reasonable request.

Author Contributions

Conceptualization, ZGuo, ZGao (equal), and XH; methodology, XN; software, XN and WZ; validation, LL, SR; formal analysis, ZGuo; investigation, QL and SF; resources, DG; data curation, LY and DG; writing—original draft preparation, ZGuo, DG and SF; writing—review and editing, ZGao and XH; visualization, LL and YL; supervision, SF; project administration, YZ and XH; funding acquisition, ZGuo, YZ, and XH. All authors have read and agreed to the published version of the manuscript. All authors contributed to editorial changes in the manuscript. All authors have participated sufficiently in the work and agreed to be accountable for all aspects of the work.

Ethics Approval and Consent to Participate

Ethical approval was granted by the Ethics Committee of the First Affiliated Hospital of Harbin Medical University (IACUC No.2025032), and this study was conducted in strict accordance with this institution's ethical guidelines and relevant national/institutional regulations for animal experimentation.

Acknowledgment

Not applicable.

Funding

This study was supported by the National Natural Science Foundation of China (No.82274028), the Heilongjiang Key R&D Program (No.2022ZX02C09), the Fundamental Research Funds for the Provincial Universities in Heilongjiang Province (2025, Zhibo Guo), Natural Science Foundation of Heilongjiang Province (No.JJ2025PL0189), the Innovation Fund of the First Affiliated Hospital of Harbin Medical University (2024M10 and 2024M25), and 2025 Central Government Fiscal Subsidy Fund for Medical Care Compliance and Capacity Enhancement (Traditional Chinese Medicine Undertakings and Inheritance and Development Component) (23000025353321000086).

Conflict of Interest

The authors declare no conflict of interest.

Supplementary Material

Supplementary material associated with this article can be found, in the online version, at https://doi.org/10.31083/FBL48584.

References

[1] Lo-Coco F, Avvisati G, Vignetti M, Thiede C, Orlando SM, Iacobelli S, *et al*. Retinoic acid and arsenic trioxide for acute promyelocytic leukemia. The New England Journal of Medicine. 2013; 369: 111–121. https://doi.org/10.1056/NEJMoa1300874.

[2] Yu PH, Zhu CY, Kang YY, Naranmandura H, Yang C. Mutation in the Unrearranged *PML* Allele Confers Resistance to Arsenic

Trioxide in Acute Promyelocytic Leukemia. Research (Washington, D.C.). 2025; 8: 0696. https://doi.org/10.34133/research.0696.

[3] Mathews V, George B, Lakshmi KM, Viswabandya A, Bajel A, Balasubramanian P, *et al*. Single-agent arsenic trioxide in the treatment of newly diagnosed acute promyelocytic leukemia: durable remissions with minimal toxicity. Blood. 2006; 107: 2627–2632. https://doi.org/10.1182/blood-2005-08-3532.

[4] Zhang D, Li Y, Liu T, Liu X, Zhang J. Efficacy and safety analysis of different treatment regimens in newly diagnosed acute promyelocytic leukemia. Annals of Hematology. 2025; 104: 3703–3711. https://doi.org/10.1007/s00277-025-06495-8.

[5] Ling S, Shan Q, Liu P, Feng T, Zhang X, Xiang P, *et al*. Metformin ameliorates arsenic trioxide hepatotoxicity via inhibiting mitochondrial complex I. Cell Death & Disease. 2017; 8: e3159. https://doi.org/10.1038/cddis.2017.482.

[6] Wang L, Liu S, Gao C, Chen H, Li J, Lu J, *et al*. Arsenic trioxide-induced cardiotoxicity triggers ferroptosis in cardiomyoblast cells. Human & Experimental Toxicology. 2022; 41: 9603271211064537. https://doi.org/10.1177/09603271211064537.

[7] Zhong G, Wan F, Lan J, Jiang X, Wu S, Pan J, *et al*. Arsenic exposure induces intestinal barrier damage and consequent activation of gut-liver axis leading to inflammation and pyroptosis of liver in ducks. The Science of the Total Environment. 2021; 788: 147780. https://doi.org/10.1016/j.scitotenv.2021.147780.

[8] Li J, Chen X, Zhao S, Chen J. Arsenic-Containing Medicine Treatment Disturbed the Human Intestinal Microbial Flora. Toxics. 2023; 11: 458. https://doi.org/10.3390/toxics11050458.

[9] Blake SJ, Wolf Y, Boursi B, Lynn DJ. Role of the microbiota in response to and recovery from cancer therapy. Nature Reviews. Immunology. 2024; 24: 308–325. https://doi.org/10.1038/s41577-023-00951-0.

[10] Wang R, Yang X, Liu J, Zhong F, Zhang C, Chen Y, *et al*. Gut microbiota regulates acute myeloid leukaemia via alteration of intestinal barrier function mediated by butyrate. Nature Communications. 2022; 13: 2522. https://doi.org/10.1038/s41467-022-30240-8.

[11] Yoon SE, Kang W, Choi S, Park Y, Chalita M, Kim H, *et al*. The influence of microbial dysbiosis on immunochemotherapy-related efficacy and safety in diffuse large B-cell lymphoma. Blood. 2023; 141: 2224–2238. https://doi.org/10.1182/blood.2022018831.

[12] Malard F, Vekhoff A, Lapusan S, Isnard F, D'incan-Corda E, Rey J, *et al*. Gut microbiota diversity after autologous fecal microbiota transfer in acute myeloid leukemia patients. Nature Communications. 2021; 12: 3084. https://doi.org/10.1038/s41467-021-23376-6.

[13] Masetti R, Leardini D, Muratore E, Fabbrini M, D'Amico F, Zama D, *et al*. Gut microbiota diversity before allogeneic hematopoietic stem cell transplantation as a predictor of mortality in children. Blood. 2023; 142: 1387–1398. https://doi.org/10.1182/blood.2023020026.

[14] Mei Y, Ren K, Liu Y, Ma A, Xia Z, Han X, *et al*. Bone marrow-confined IL-6 signaling mediates the progression of myelodysplastic syndromes to acute myeloid leukemia. The Journal of Clinical Investigation. 2022; 132: e152673. https://doi.org/10.1172/JCI152673.

[15] Xu S, Wang S, Xing S, Yu D, Rong B, Gao H, *et al*. KDM5A suppresses PML-RARα target gene expression and APL differentiation through repressing H3K4me2. Blood Advances. 2021; 5: 3241–3253. https://doi.org/10.1182/bloodadvances.2020002819.

[16] Li H, Ye F, Li Z, Peng X, Wu L, Liu Q. The response of gut microbiota to arsenic metabolism is involved in arsenic-induced liver injury, which is influenced by the interaction between arsenic and methionine synthase. Environment International. 2024; 190: 108824. https://doi.org/10.1016/j.envint.2024.108824.

[17] Chen B, Khodadoust MS, Liu CL, Newman AM, Alizadeh AA. Profiling Tumor Infiltrating Immune Cells with CIBERSORT. Methods in Molecular Biology (Clifton, N.J.). 2018; 1711: 243–259. https://doi.org/10.1007/978-1-4939-7493-1_12.

[18] Cao F, Jin L, Gao Y, Ding Y, Wen H, Qian Z, *et al*. Artificial-enzymes-armed Bifidobacterium longum probiotics for alleviating intestinal inflammation and microbiota dysbiosis. Nature Nanotechnology. 2023; 18: 617–627. https://doi.org/10.1038/s41565-023-01346-x.

[19] Nan K, Zhong Z, Yue Y, Shen Y, Zhang H, Wang Z, *et al*. Fasting-mimicking diet-enriched *Bifidobacterium pseudolongum* suppresses colorectal cancer by inducing memory $CD8^+$ T cells. Gut. 2025; 74: 775–786. https://doi.org/10.1136/gutjnl-2024-333020.

[20] Zhao Q, Guo M, Hostetter TH, Chen H, Lin L, Hai X. Effect of renal impairment on arsenic accumulation, methylation capacity, and safety in acute promyelocytic leukemia (APL) patients treated with arsenic trioxide. Expert Review of Clinical Pharmacology. 2021; 14: 1173–1182. https://doi.org/10.1080/17512433.2021.1938549.

[21] Cicconi L, Divona M, Ciardi C, Ottone T, Ferrantini A, Lavorgna S, *et al*. PML-RARα kinetics and impact of FLT3-ITD mutations in newly diagnosed acute promyelocytic leukaemia treated with ATRA and ATO or ATRA and chemotherapy. Leukemia. 2016; 30: 1987–1992. https://doi.org/10.1038/leu.2016.122.

[22] Bercier P, Wang QQ, Zang N, Zhang J, Yang C, Maimaitiyiming Y, *et al*. Structural Basis of PML-RARA Oncoprotein Targeting by Arsenic Unravels a Cysteine Rheostat Controlling PML Body Assembly and Function. Cancer Discovery. 2023; 13: 2548–2565. https://doi.org/10.1158/2159-8290.CD-23-0453.

[23] Maimaitiyiming Y, Wang QQ, Hsu CH, Naranmandura H. Arsenic induced epigenetic changes and relevance to treatment of acute promyelocytic leukemia and beyond. Toxicology and Applied Pharmacology. 2020; 406: 115212. https://doi.org/10.1016/j.taap.2020.115212.

[24] Lv J, Wu M, Pang C, Duan R, Zhang H, Tian S, *et al*. Torsemide increases arsenic concentrations by inhibition of multidrug resistance protein 4 in arsenic trioxide treated acute promyelocytic leukemia patients. Biomedicine & Pharmacotherapy = Biomedecine & Pharmacotherapie. 2023; 163: 114858. https://doi.org/10.1016/j.biopha.2023.114858.

[25] Iriyama N, Yuan B, Yoshino Y, Hatta Y, Horikoshi A, Aizawa S, *et al*. Aquaporin 9, a promising predictor for the cytocidal effects of arsenic trioxide in acute promyelocytic leukemia cell lines and primary blasts. Oncology Reports. 2013; 29: 2362–2368. https://doi.org/10.3892/or.2013.2388.

[26] Li M, Han X, Sun L, Liu X, Zhang W, Hao J. Indole-3-acetic acid alleviates DSS-induced colitis by promoting the production of R-equol from *Bifidobacterium pseudolongum*. Gut Microbes. 2024; 16: 2329147. https://doi.org/10.1080/19490976.2024.2329147.

[27] Melcher C, Yu J, Duong VHH, Westphal K, Helmi Siasi Farimany N, Shaverskyi A, *et al*. B cell-mediated regulatory mechanisms control tumor-promoting intestinal inflammation. Cell Reports. 2022; 40: 111051. https://doi.org/10.1016/j.celrep.2022.111051.

[28] Mazziotta F, Biavati L, Rimando J, Rutella S, Borcherding N, Parbhoo S, *et al*. CD8+ T-cell differentiation and dysfunction inform treatment response in acute myeloid leukemia. Blood. 2024; 144: 1168–1182. https://doi.org/10.1182/blood.2023021680.

[29] Zhou H, Jia B, Annageldiyev C, Minagawa K, Zhao C, Mineishi S, *et al*. $CD26^{low}PD\text{-}1^+$ CD8 T cells are terminally exhausted

and associated with leukemia progression in acute myeloid leukemia. Frontiers in Immunology. 2023; 14: 1169144. https://doi.org/10.3389/fimmu.2023.1169144.

[30] Desai PN, Wang B, Fonseca A, Borges P, Jelloul FZ, Reville PK, *et al*. Single-Cell Profiling of CD8+ T Cells in Acute Myeloid Leukemia Reveals a Continuous Spectrum of Differentiation and Clonal Hyperexpansion. Cancer Immunology Research. 2023; 11: 1011–1028. https://doi.org/10.1158/2326-6066.CIR-22-0961.

[31] Mahadevan KK, LeBleu VS, Ramirez EV, Chen Y, Li B, Sockwell AM, *et al*. Elimination of oncogenic KRAS in genetic mouse models eradicates pancreatic cancer by inducing FAS-dependent apoptosis by CD8^{+} T cells. Developmental Cell. 2023; 58: 1562–1577.e8. https://doi.org/10.1016/j.devcel.2023.07.025.

[32] van der Leun AM, Traets JJH, Vos JL, Elbers JBW, Patiwael S, Qiao X, *et al*. Dual Immune Checkpoint Blockade Induces Analogous Alterations in the Dysfunctional CD8+ T-cell and Activated Treg Compartment. Cancer Discovery. 2023; 13: 2212–2227. https://doi.org/10.1158/2159-8290.CD-22-0851.

[33] Zhang J, Li J, Hou Y, Lin Y, Zhao H, Shi Y, *et al*. Osr2 functions as a biomechanical checkpoint to aggravate CD8^{+} T cell exhaustion in tumor. Cell. 2024; 187: 3409–3426.e24. https://doi.org/10.1016/j.cell.2024.04.023.

[34] Braun DA, Wu CJ. Tumor-Infiltrating T Cells - A Portrait. The New England Journal of Medicine. 2022; 386: 992–994. https://doi.org/10.1056/NEJMcibr2119477.

[35] Stress response in tumor-infiltrating T cells is linked to immunotherapy resistance. Nature Medicine. 2023; 29: 1336–1337. https://doi.org/10.1038/s41591-023-02370-z.

[36] Zheng L, Qin S, Si W, Wang A, Xing B, Gao R, *et al*. Pan-cancer single-cell landscape of tumor-infiltrating T cells. Science (New York, N.Y.). 2021; 374: abe6474. https://doi.org/10.1126/science.abe6474.

[37] Xu G, Guo J, Fan S, Li S, Qiu T, Chen Z, *et al*. Single-cell omics analysis reveals tumor microenvironment rewiring after arsenic trioxide therapy in acute promyelocytic leukemia. Science Bulletin. 2025. https://doi.org/10.1016/j.scib.2025.09.014. (online ahead of print)

[38] Ugel S, Canè S, De Sanctis F, Bronte V. Monocytes in the Tumor Microenvironment. Annual Review of Pathology. 2021; 16: 93–122. https://doi.org/10.1146/annurev-pathmechdis-012418-013058.

[39] Zaric M, Becker PD, Hervouet C, Kalcheva P, Doszpoly A, Blattman N, *et al*. Skin immunisation activates an innate lymphoid cell-monocyte axis regulating CD8^{+} effector recruitment to mucosal tissues. Nature Communications. 2019; 10: 2214. https://doi.org/10.1038/s41467-019-09969-2.